3D NUMERICAL STUDY OF AIRFLOW IN THE COMPRESSOR/COMBUSTOR PREDIFFUSER AND DUMP DIFFUSER OF AN INDUSTRIAL GAS TURBINE

Ajay K. Agrawal* and Tah-teh Yang
Department of Mechanical Engineering
Clemson University, Clemson, SC 29631-0921

SUMMARY

This paper describes the 3D computations of a flow field in the compressor/combustor diffusers of an industrial gas turbine. The geometry considered includes components such as the combustor support strut, the transition piece and the impingement sleeve with discrete cooling air holes on its surface. Because the geometry was complex and 3D, the airflow path was divided into two computational domains sharing an interface region. The body-fitted grid was generated independently in each of the two domains. The governing equations for incompressible Navier-Stokes equations were solved using the finite volume approach. The results show that the flow in the prediffuser is strongly coupled with the flow in the dump diffuser and vice versa. The computations also revealed that the flow in the dump diffuser is highly nonuniform.

INTRODUCTION

In gas turbine engines the air exiting the compressor is decelerated in the annular prediffuser before it is discharged into the dump diffuser. The dump diffuser then distributes the air to the combustor(s) through the annular jacket(s). Typical aircraft engines use an annular combustor, which extends over 360 degrees continuously around the turbine axis. In contrast, the industrial gas turbines use several can combustors discretely and equispaced in the circumferential direction. Each of these combustor cans has an annular jacket around it which receives air from the dump diffuser and then feeds it to the combustor can for combustion.

From the gas turbine's compressor exit to the combustor, frictional losses in the diffuser flow path adversely affect the efficiency of the gas turbine. The diffuser system must uniformly distribute air to the hot-sections of the turbine to maintain combustion, to improve thermal mixing and to avoid local burnout. Thus, high efficiency advanced gas turbines require an aerodynamic design of the prediffuser and dump diffuser for minimizing energy losses and for maintaining combustion stability and performance. The design of these flow systems is complicated because of two main reasons (1) the performance of the prediffuser is affected by the flow

* Present Address:
School of Aerospace and Mechanical Engineering
The University of Oklahoma, Norman, OK 73019-0601

conditions in the dump region and vice versa and (2) the flow geometry in the dump region is 3D. The complex geometry and the flow interactions between the components of the compressor/combustor region present a significant design challenge.

The test model in figure 1 depicts the air flow path in the compressor/combustor region of an industrial gas turbine. After passing through the annular prediffuser, a portion of the air flows through the cooling holes in the impingement sleeve into the space between the impingement sleeve and the transition piece; then it flows through this annular space towards the combustor can and finally mixes with the balance of the air flowing through the bypass air ports. Next, the air enters the combustor can through primary, secondary, dilution and cooling holes. Several components in the flow path disrupt the circumferential uniformity; hence, the resulting flow field is 3D. The authors of this study are aware of only one other similar investigation, which was conducted by Karki et al. (ref. 1). Their investigation considered a typical combustor-diffuser in aircraft engines. The diffuser geometry and the flow path in the present study are far more complex than that in the study by Karki et al (ref. 1).

The primary purpose of this work was to simulate the cold airflow in the test model of an industrial gas turbine. Thus, the reacting flow in the combustor can and the hot-gas flow through the transition piece were not considered. However, the geometric details of the transition piece and the surrounding impingement sleeve were included to add realism to the simulations. In computations, the airflow exited at the annular space between the combustor casing and the combustor can. In the circumferential direction, the exact same geometry of the combustor/transition piece assembly repeats cyclically. Additionally, each of these assemblies is symmetric about its midplane. Therefore, the computations in the circumferential direction were required in only one-half of the distance between the adjacent combustor/transition piece assemblies (which is 1/28th of the full 360 degrees).

COMPUTATIONAL PROCEDURE

Because the geometry was complex and 3D, the airflow path was divided into two computational domains. The lower domain included the prediffuser, a part of the combustor support strut and the lower dump diffuser. The upper domain included the details of the combustor/transition piece assembly, the upper dump diffuser and a part of the combustor support strut. These two domains shared an interface region through which boundary condition data were communicated between the two domains and updated during the computations.

Grid Generation

The body-fitted, curvilinear coordinate system was used to incorporate the geometric details in the computational analysis. Internal solid objects, such as the support struts and the surface of the impingement sleeve were, simulated by blocking the flow through the grids representing these areas. Figure 2 shows the computational grid in the two domains on a longitudinal

plane between the combustor support struts and also the midplane of the combustor/transition piece assembly. The shaded grids in figure 2 were impervious to the flow. Thus, they represent internal solid objects, such as the impingement sleeve and the transition piece. The procedure for generating the 3-D computational grid is described below.

EasyMesh-3D, a 3-D mesh-generation program (ref. 2), was used to independently generate a structured grid in each of the two domains. First, the computational domain was divided into subsections or subvolumes. These subvolumes represented specific objects inside the computational domains. The mesh was generated within each subvolume, which allowed local grid refinement and accurate representation of flow obstructions. The computational grid in the lower domain consisted of 62,208 grids with 18 in the circumferential direction, 32 in the radial direction and 108 in the axial direction.

The computational grid in the upper domain represented the complex 3-D shape of the combustor/transition piece and the combustor casing/impingement sleeve. The combustor and its casing are circular in cross-section. The transition piece and impingement sleeve are circular at the combustor end and are nearly rectangular at the turbine inlet. Moreover, the spacing between the adjacent combustor/transition piece assemblies varies along the axial direction. This spacing is maximum at the combustor end and zero at the turbine inlet. The computational grid on the surface of the combustor can/transition piece is shown in figure 3. The mesh was constructed by prescribing geometric details at 5 axial locations. Azimuthal planes at each of these axial locations were divided into 6 subsections. Therefore, a total of 30 subvolumes formed the upper computational domain. Figures 3 and 4 show, respectively, the azimuthal planes at the combustor exit and the turbine inlet. As seen in figures 4 and 5, the surface of the impingement sleeve was broken into three segments, each of which belonged to a subsection. This procedure allowed flexibility in generating the mesh and improved grid resolution and grid orthogonality. Figures 4 and 5 identify also the grids that were blocked to the flow and that represent the solid objects. The computational grid in the upper domain consisted of 63,648 grids with 18 in the circumferential direction, 52 in the radial direction and 68 in the axial direction.

In the test model, the air enters the space between the impingement sleeve/transition piece and the combustor casing/combustor through cooling air holes on the impingement sleeve and the bypass air holes on the combustor casing. The combustor casing has 3 rows of bypass air holes, and each of these rows consists of several discrete holes equally spaced in the circumferential direction. The impingement sleeve has several rows of smaller cooling air holes. The finite grid in the present analysis could not precisely and indivisibly resolve the large number of cooling holes. Therefore, only 12 holes were considered in each row. These holes were distributed nearly uniformly in the circumferential direction. Although the exact shape and orientation of the holes in a row could differ, the area of each hole was kept the same. If the actual number of holes in a row exceeded 12, then the total area of these 12 holes was made to equal the actual total area of the holes in that row. Each hole comprised of at least 1 or more grids. When the area of a grid exceeded the area of the hole it represented, the grid was partially blocked to the flow.

Because the mesh was generated independently in each of the two domains, the grids differ at the interface between these domains. Linear interpolation was used to compute boundary data at the proper interface location before the information was transferred from from one domain to another.

Governing Equations

Using Cartesian tensor notation, governing equations for incompressible turbulent flow are expressed in time-averaged form:

$$\frac{\partial}{\partial x_j}(\rho V_j) = 0 \tag{1}$$

$$\frac{\partial}{\partial x_j}(\rho V_j V_i) = -\frac{\partial p}{\partial x_i} + \frac{\partial}{\partial x_j}\left[\mu_{eff}\frac{\partial V_i}{\partial x_j}\right] \tag{2}$$

The effective viscosity, μ_{eff}, was defined by the relation

$$\mu_{eff} = \mu + \mu_t \tag{3}$$

The turbulent viscosity, μ_t, in equation (3) was obtained from the standard k-ε model of turbulence.

Boundary Conditions

Because of the symmetry, the mass flow rate and the gradients of dependent variables were specified as zero at the two circumferential boundaries.

Inlet.-- In the lower domain, the axial velocity at the inlet of the prediffuser was prescribed according to the measured data. Inlet radial and circumferential velocities were assumed to be zero. The inlet turbulence intensity was taken as 10%. The inlet turbulent energy dissipation was calculated from

$$\varepsilon = [C_D^{0.75} k^{1.5}]/\ell \tag{4}$$

where the length scale, ℓ, was the annular gap. The axial diffusion at the prediffuser inlet was ignored.

The interface between the domains was also the inlet to the upper domain. Values of all the dependent variables at the inlet to the upper domain were determined from flow computations in the lower domain. The diffusion at the interface was neglected.

Walls.-- The wall function approach for turbulent flow was employed. This approach requires that the logarithmic velocity profile bridge the region between a wall and a near wall node on the outside of the viscous sublayer. Turbulence in the near wall region was in local equilibrium.

Outlet.-- The fluid leaves the upper domain through the annular gap between the combustor and the combustor casing. A constant static pressure was specified at this outlet. The axial diffusion at the outlet was ignored.

The interface between the domains was also the outlet to the lower domain. The static pressure at this outlet was determined from flow computations in the upper domain. The radial diffusion at the interface was neglected.

Solution Procedure

The governing equations for each dependent variable could be reduced to a single general form:

$$\nabla \cdot (\rho V\phi + J_\phi) = S_\phi \qquad (5)$$

where ϕ represents the dependent variable, V is the velocity vector, J_ϕ is the diffusive flux vector ($-\Gamma_\phi \nabla\phi$) and S_ϕ is the volumetric source of ϕ. Integration of the generalized equation (5) over control volumes resulted in the finite difference equations of a general form. Convection-diffusion terms in the governing equations were discretized using the upwind scheme. The set of coupled nonlinear equations was solved implicitly in an iterative manner. Coupling between velocity and pressure fields was provided by a variant of the SIMPLE algorithm (ref. 3) called SIMPLEC.

The computational steps to implement the subdomain procedure can be described as follows:

(1) Prescribe a guess pressure distribution at the outlet of the lower domain (or the interface)
(2) Compute the flow field in the lower domain
(3) Compute the flow field in the upper domain. The flow solution in the lower domain provides boundary condition data at the inlet to the upper domain (or the interface).
(4) Return to step 2 with an updated guess for the pressure distribution at the interface obtained from the solution in the upper domain. Continue these trials until the pressure distribution at the interface no longer changes.

It was necessary to underrelax the changes in the pressure distribution at the interface. Underrelaxing prevented large differences between the successive updates of the pressure field at the interface which otherwise led to oscillations. In the present work, an underrelaxation value of 0.2 was used. The computations proceeded serially on a single CPU. Thus, at the end of computations in a domain, both geometric and flow field data were saved on disk files before computations were initiated for another domain. Each trial took approximately 120 flow iterations. The flow field calculated for an earlier trial served as the initial guess for the new trial. The flow field converged after 6 to 10 trials. Each trial took 6 to 8 CPU hours on a Sun Sparkstation 10 Model 30.

RESULTS AND DISCUSSIONS

Flow Field

The computed flow field at the midplane of the combustor/transition piece assembly (also in between the combustor support struts) is shown in Figure 6. The air in the prediffuser's outer region accelerates as it exits the prediffuser. Then, it turns almost 180 degrees to enter the bypass air holes on the combustor casing. This short-circuiting of the diffuser flow is referred to as the sink effect of the combustor bypass air holes on the flow field in the pre- and dump diffusers. Flow acceleration is detrimental to a diffuser's performance because the primary function of a diffuser is to diffuse or decelerate the flow.

The flow separates underneath the impingement sleeve close to the turbine inlet. Nearly half the distance between the prediffuser exit and the turbine inlet is occupied by the recirculating flow. The flow separates also in the lower dump diffuser at the tip of the prediffuser's outer wall and in the space between the combustor casing and the prediffuser's outer wall. However, the size and strength of these eddies are relatively small. All recirculating flows dissipate the energy received from the main flow, thus contributing to frictional losses.

The flow field at the midplane of the strut and also in between the combustor/transition piece assembly is shown in Figure 7. The combustor support strut completely blocks the prediffuser flow, which is then redirected in the circumferential direction. Thus, the flow in the pre- and dump diffusers is 3-D. The flow remains separated underneath the impingement sleeve near the turbine inlet.

Figures 8 and 9 show projections of velocity vectors on axial planes P1 and P2 identified in Figure 6. At plane P1 (figure 8), the support struts block a large portion of the flow area, and the impingement sleeve is nearly circular in cross-section. The fluid underneath the support struts turns azimuthally before joining the fluid flowing towards the impingement sleeve. Fluid velocity near the side panel (3 or 9 o'clock position) of the impingement sleeve is high while that near the outer panel (12 o'clock position) is relatively small. Thus, the outer region of the dump diffuser behaves as a large reservoir. At plane P2, the blockage due to the support strut is reduced, and the impingement sleeve is nearly rectangular in cross-section. The flow field at

plane P2, shown in Figure 9, is similar to that at plane P1, except that the fluid velocity near the side panel is even higher because of the smaller gap between the adjacent impingement sleeves.

Overall System Performance

Performance Parameters.-- At any plane the mass flow rate, $\dot{m}$ was obtained as

$$\dot{m} = \int \rho u \, dA = \rho \bar{u} A \tag{6}$$

where u is the velocity component perpendicular to the flow area.

The mass-averaged pressures at a plane were derived as

$$\bar{P} = \frac{1}{\dot{m}} \int P \rho u \, dA \tag{7}$$

and

$$\bar{p} = \frac{1}{\dot{m}} \int p \rho u \, dA \tag{8}$$

where P and p are the local total and static pressures, respectively.

The total pressure P at a point is related to the static pressure p at that point as

$$P = p + 0.5 \rho V^2 \tag{9}$$

where V is the total velocity at that point.

The wall static pressure recovery coefficient (C_p) and the total pressure loss coefficient (λ) are defined as

$$C_p = [p - \bar{p}_a]/h_d \tag{10}$$

and

$$\lambda_{a\text{-}c} = [\bar{P}_c - \bar{P}_a]/h_d \tag{11}$$

where h_d is the dynamic head at the prediffuser inlet $[\bar{P}_a - \bar{p}_a]$.

Prediffuser Wall Static Pressure Recovery.-- Figure 10 shows the static pressure recovery coefficients along the inner and outer walls of the prediffuser. The pressure increases linearly along the inner wall of the prediffuser, and a C_p of nearly 0.6 is reached at the prediffuser exit.

The prediffuser outer wall C_p is nearly zero owning to the flow acceleration at the prediffuser exit because of the sinkeffect.

Because the prediffuser flow is highly coupled with the flow in the dump diffuser, the wall pressure recovery coefficients may not appropriate performance parameters. The mass-averaged total pressure loss coefficients presented below provide a quantitative description of the prediffuser performance.

Total Pressure Loss.-- The mass-weighted total pressure loss coefficients in the diffuser systems are summarized in Table 1. The computations indicate that more than 1 dynamic head at the prediffuser inlet (or the compressor discharge) is lost in the diffusers. Approximately 80% of this loss occurs in the upper dump diffuser where the fluid must pass through the narrow gaps and pathways between the adjacent combustor/transition piece assemblies. The total pressure loss in the prediffuser is relatively small: only 3% of the total pressure loss in the diffusers. The remaining 17% of the pressure loss occurs in the lower dump diffuser.

Flow Uniformity around the Impingement Sleeve

Figure 11 shows the static pressure distributions along the impingement sleeve at 3 circumferential locations: 12 o'clock, 3 o'clock and 6 o'clock. The reference pressure in Figure 11 is the static pressure at a point on the 12 o'clock position. Figure 11 shows that the static pressure varies both along the length and the periphery of the sleeve. The pressure is highest at the 6 o'clock position and is lowest at the 3 o'clock position. At the 12 o'clock position, the pressure is nearly constant along the length of the sleeve, indicating that the outer most dump diffuser behaves as a plenum. At the 3 o'clock position (or the side panel), the pressure decreases along the length of the sleeve because of the increased venturi effect induced by a smaller space between adjacent sleeves. Three-D computations indicate reverse flow from the side panel. When the reverse flow occurs, the air exits into the dump diffuser through cooling holes on the impingement sleeve.

REFERENCES

1. Karki, K.C., Oechsle, V.L., and Mongia, H.C., "A Computational Procedure for Diffuser-Combustor Flow Interaction Analysis," ASME Paper No. 90-GT-35, 1990.
2. CFD2000 User Manual, Adaptive Research Corporation, Huntsville, Alabama, 1992.
3. Patankar, S.V., Numerical Heat Transfer and Fluid Flow, Hemisphere, 1980.

Table 1. Mass-Averaged Pressure Loss Coefficient

Prediffuser	0.04 (3%)
Dump Diffuser	
Lower Part	0.22 (19%)
Upper Part	0.93 (78%)
Total	1.19 (100%)

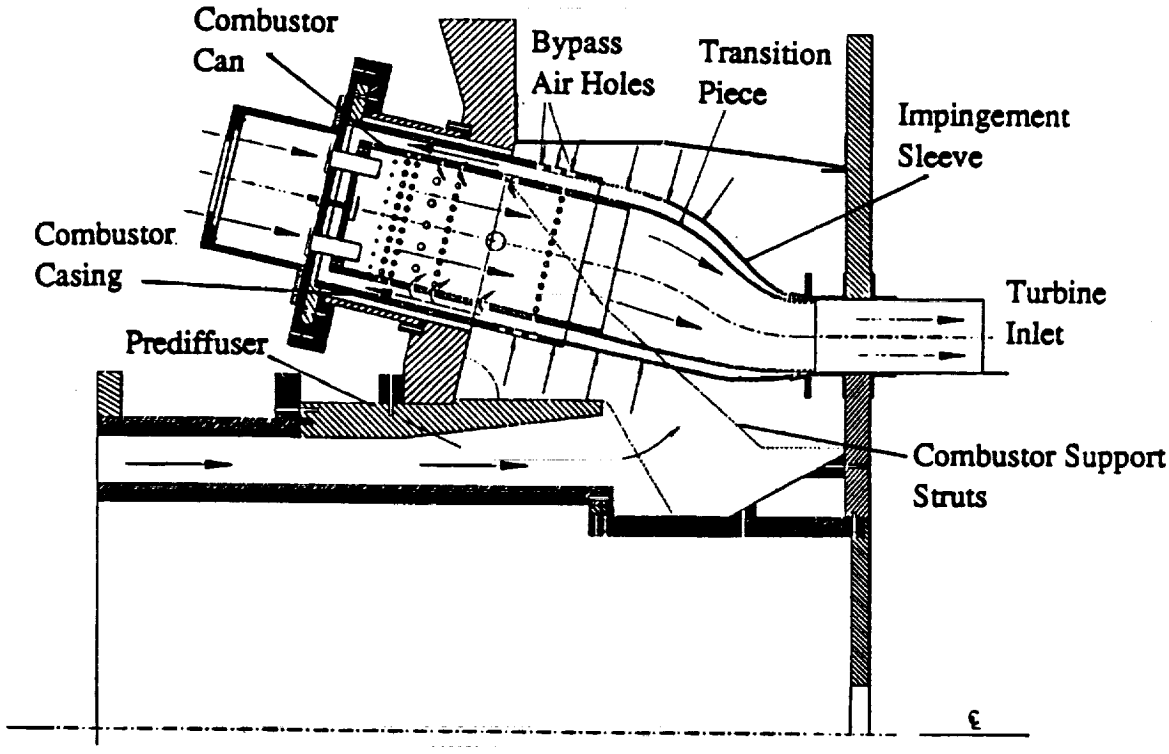

Figure 1. Airflow Path in the Compressor/Combustor Region of an Industrial Gas Turbine

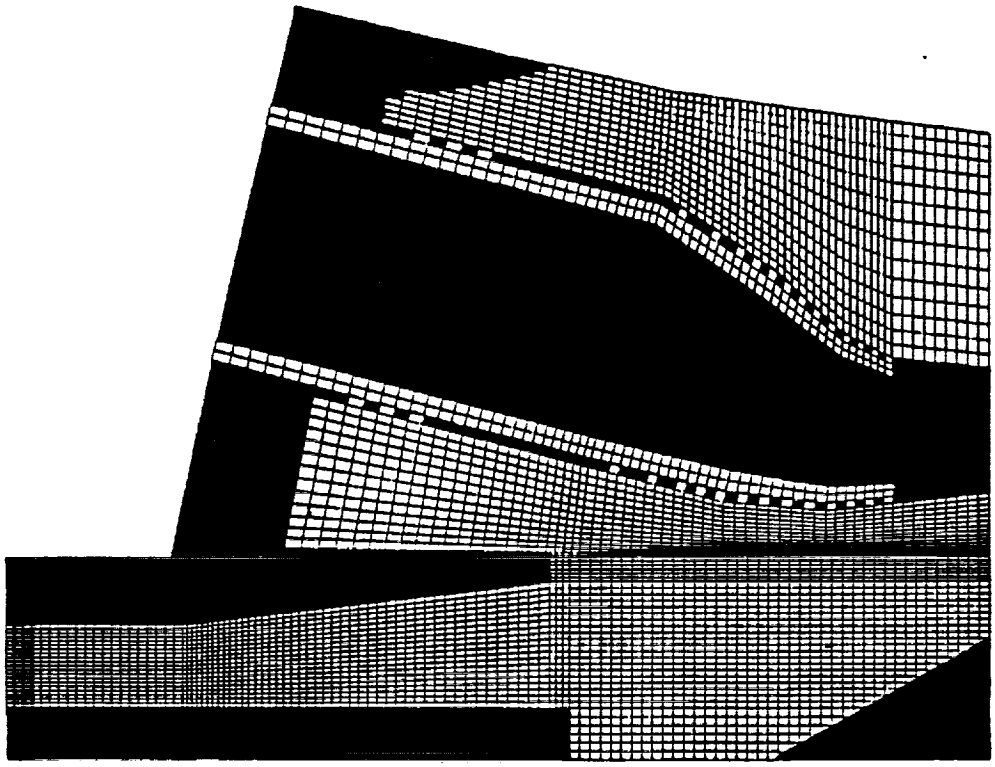

Figure 2. Computational Grid in the Two Domains
(Between the Combustor Support Struts)

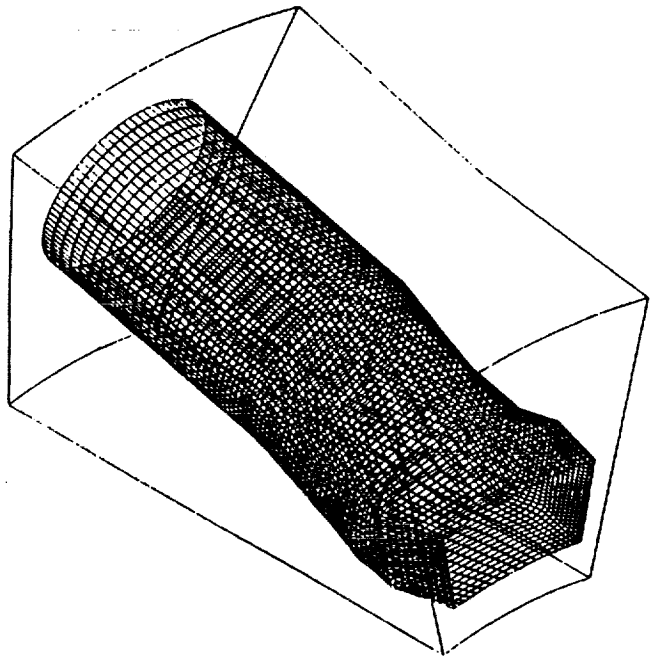

Figure 3. Computational Grid on the Surface of the Impingement Sleeve

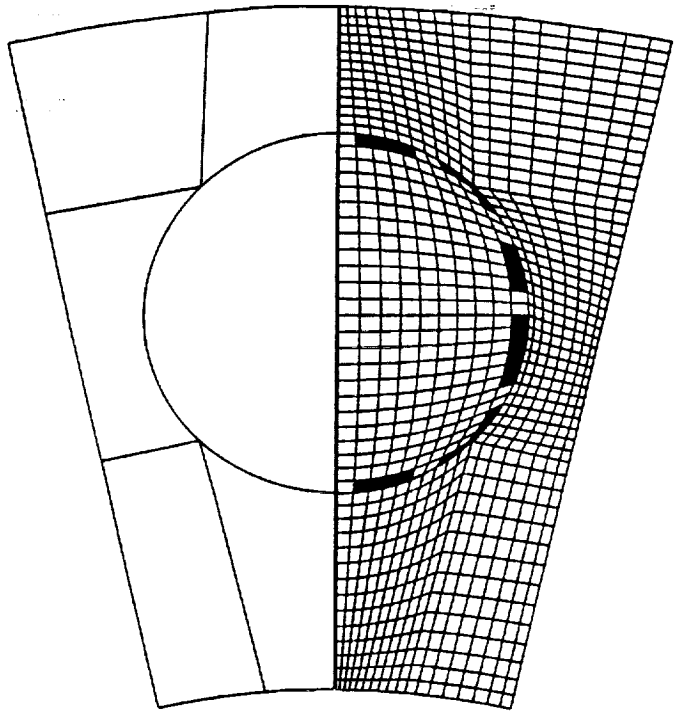

Figure 4. Upper Computational Domain Divided into 6 Subvolumes
(Azimuthal Plane Near the Combustor Can)

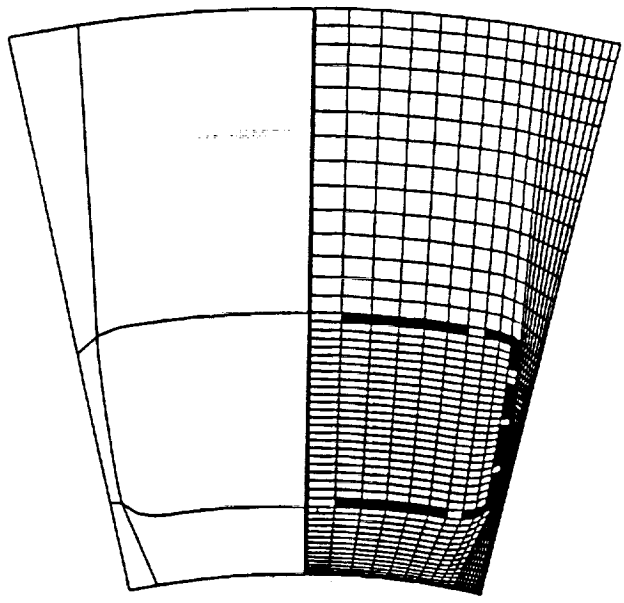

Figure 5. Upper Computational Domain Divided into 6 Subvolumes
(Azimuthal Plane Near the Turbine Inlet)

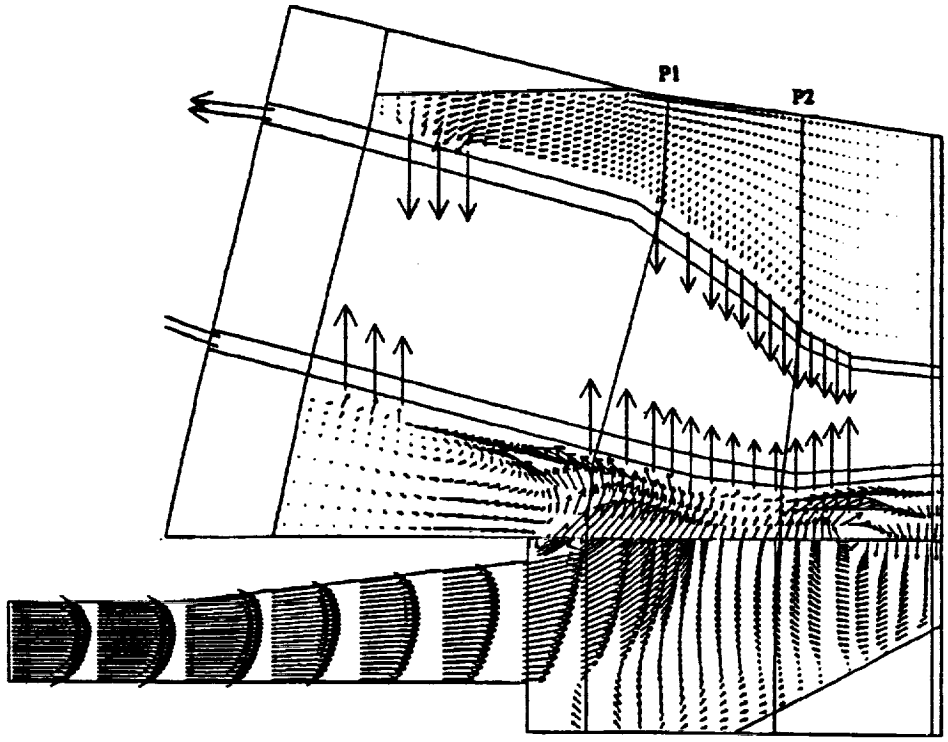

Figure 6. Velocity Vectors on a Longitudinal Plane
(Between the Combustor Support Struts)

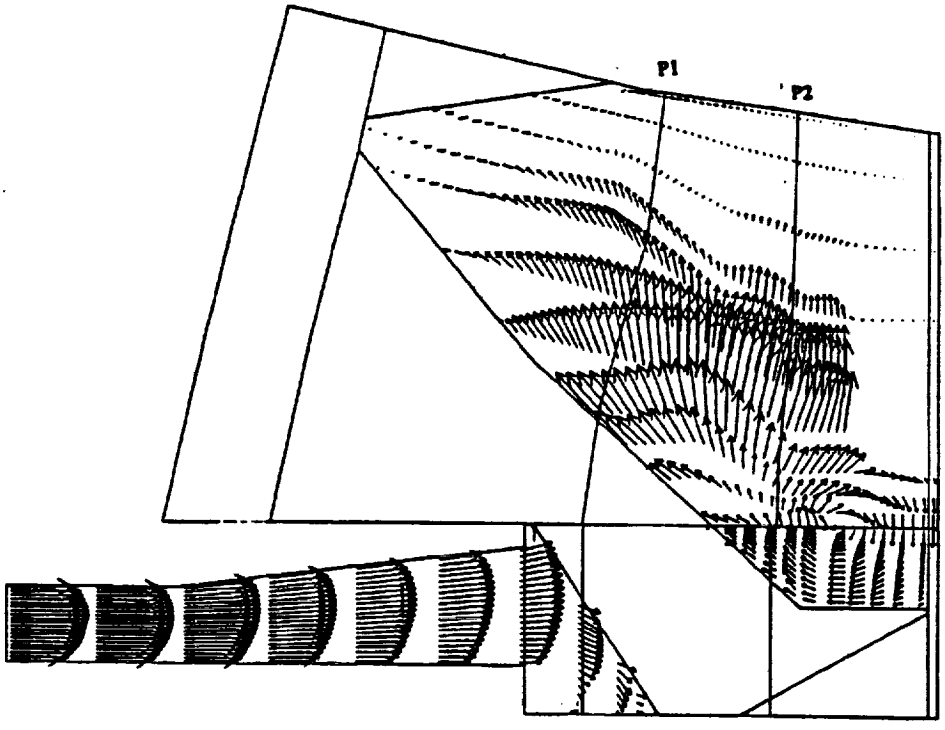

Figure 7. Velocity Vectors on a Longitudinal Plane
(Midplane of the Combustor/Transition Piece Assembly)

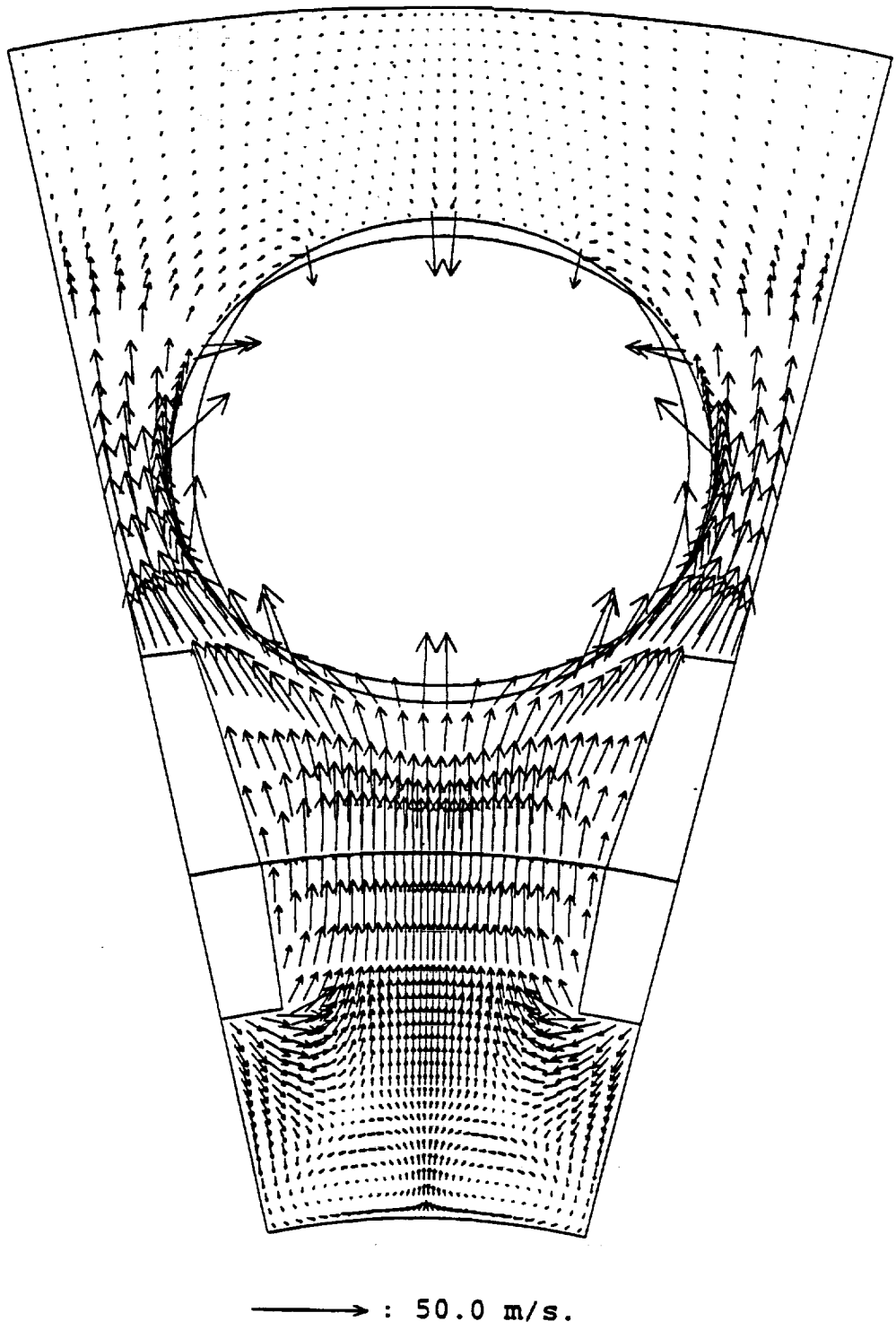

Figure 8. Velocity Vectors on an Azimuthal Plane
(Axial Location P1)

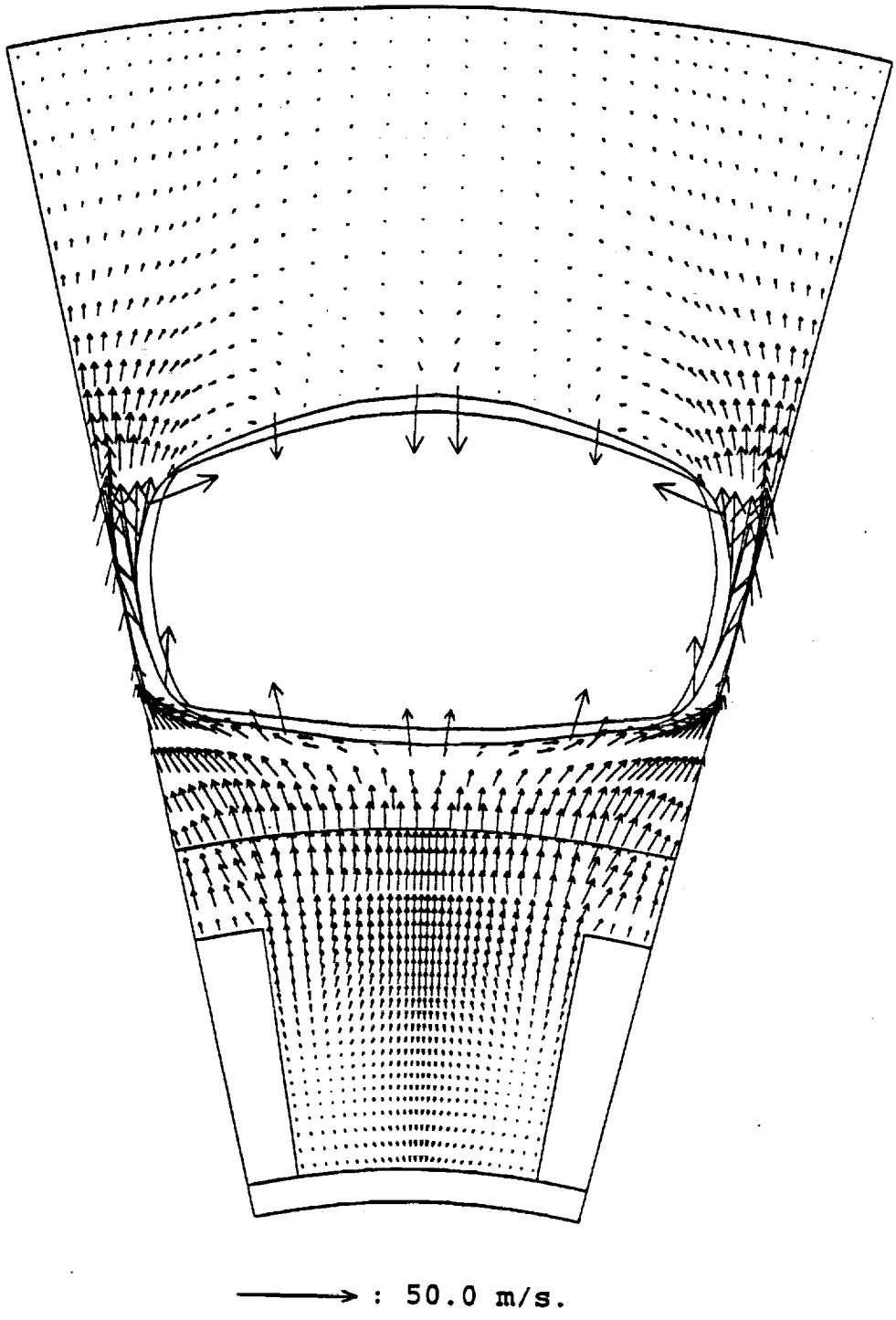

Figure 9. Velocity Vectors on an Azimuthal Plane
(Axial Location P2)

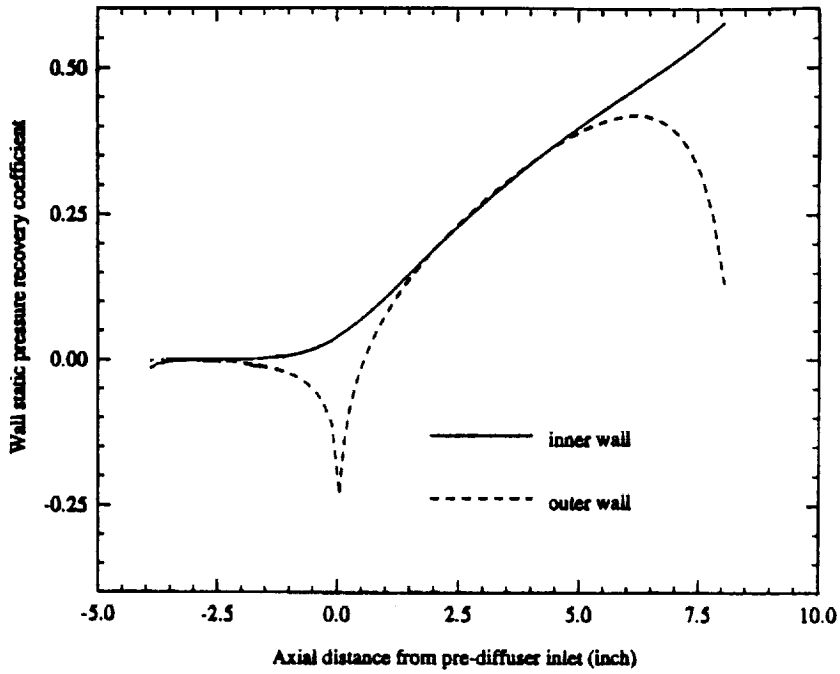

Figure 10. Prediffuser Wall Static Pressure Recovery Coefficients

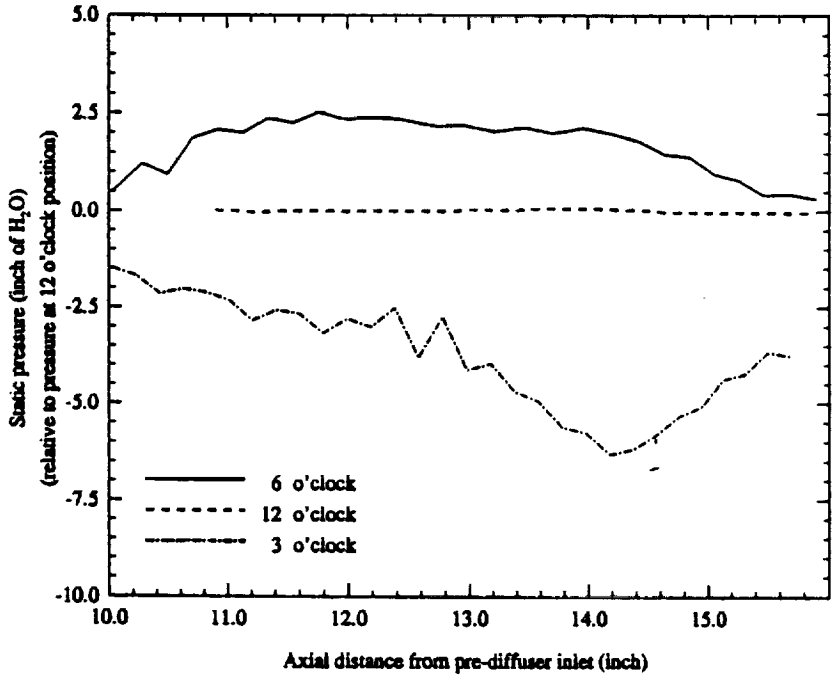

Figure 11. Static Pressure Distribution Along the Impingement Sleeve

Session Five

Multiphase Flow